RSC Advances

This is an *Accepted Manuscript*, which has been through the Royal Society of Chemistry peer review process and has been accepted for publication.

Accepted Manuscripts are published online shortly after acceptance, before technical editing, formatting and proof reading. Using this free service, authors can make their results available to the community, in citable form, before we publish the edited article. This *Accepted Manuscript* will be replaced by the edited, formatted and paginated article as soon as this is available.

You can find more information about *Accepted Manuscripts* in the Information for Authors.

Please note that technical editing may introduce minor changes to the text and/or graphics, which may alter content. The journal's standard Terms & Conditions and the Ethical guidelines still apply. In no event shall the Royal Society of Chemistry be held responsible for any errors or omissions in this *Accepted Manuscript* or any consequences arising from the use of any information it contains.

ROYAL SOCIETY OF CHEMISTRY

www.rsc.org/advances

RSC Advances

RSCPublishing

ARTICLE

Fabrication of Nanoprotrusion Surface Structured Silica Nanofibers for Improvement of Toughening of Polypropylene

Cite this: DOI: 10.1039/xoxxoooooox

Yongri Liang[a*], Shipeng Wen[c], Yanyan Ren[c], and Li Liu[b*]

Received 00th January 2012,
Accepted 00th January 2012

DOI: 10.1039/x0xx00000x

www.rsc.org/

Toughening of semi-crystalline polymer with inorganic nanofiller is very important in the practical applications. In this work, we successfully fabricated surface attaching silica nanoparticles of silica nanofibers (SiO_2@SNFs) from calcination of electrospun poly (vinyl pyrrolidone)/tetraethyl orthosilicate/silica nanoparticle (PVP/TEOS/SiO_2) nanofibers for toughening of polypropylene (PP). The SiO_2@SNFs had nanoprotrusion structured surface, and the degree of surface nanoprotrusion of silica nanofiber (SNF) can be adjusted via the incorporated SiO_2 nanoparticles content of SiO_2@SNFs. Effects of the SiO_2 content of SiO_2@SNFs on the crystallization behavior, the relative β-form crystal content, and mechanical properties of PP were investigated with polarized optical microscopy, X-ray diffraction and notched Izod impact test methods. By comparison with SNF, the SiO_2@SNFs showed better improvement of impact strength and heterogeneous crystal nucleation for PP at same loading content of filler. The impact strength of PP/SiO_2@SNFs at loading 2wt% of SiO_2@SNFs with 9 phr (SiO_2/TEOS=9/100) of SiO_2 nanoparticles was improved about 1.9 and 1.4 times than that of neat PP and PP/SNFs composite (2wt% of SNFs), respectively. However, the crystallinity, the relative β-form crystal content, and tensile strength of PP/SiO_2@SNFs were almost independent of the SiO_2 nanoparticles content of SiO_2@SNFs. Our results demonstrated that the nanoprotrusion surface structured silica nanofibers can be used as a novel nanofiller for improving the toughening of PP.

Introduction

Toughening of semi-crystalline polymer with inorganic nanofiller is very important in the practical applications.[1, 2] Isotactic polypropylene (iPP) is one of important commodity semi-crystalline polymers and widely used as matrix component in automotive parts, appliances and other industrial uses. iPP has a lot of good properties such as processability, chemical resistance, low density, and low price etc. However, the poor impact strength of iPP at low temperature limits its applications. Therefore, toughness of iPP is very important in most practical applications. [3-11]

In general, rubber toughening of iPP is one of effective methods to improve the impact strength. However, the significant drawback of rubber toughneing of iPP is the expense of the tensile strength and Young's modulus. [3, 12] There is considerable interest to simultaneously improve both the stiffness and toughness of semi-crystalline polymers. Recently, numerous researchers reported that the toughening of iPP can be achieved by incorporation of inorganic nanoparticles, such as micrometer or nanometer scale of calcium carbonate ($CaCO_3$)[5, 6, 8, 13-15], silica (SiO_2) nanoparticles[1], graphene oxide (GO)[9], glass fiber (GF)[10], fly ash[11] etc. For example, Lin et al.[15] reported that the average Izod impact strength of the 150 °C-annealed nanocomposite, containing 20 wt % (7.8 vol %) $CaCO_3$ nanoparticles coated with 6 wt % stearic acid, was 168 J/m (3.5 times higher than that of iPP). Thio et al. [14] investigated the mechanisms of deformation and fracture of iPP/$CaCO_3$ composites with various diameters of $CaCO_3$ (0.07, 0.7, and 3.5 μm). They found that incorporation of 0.7 μm $CaCO_3$ particles into iPP matrix led to an improvement in the Izod impact strength of iPP by up to four times. Li and Dou[13] investigated the influence of malonic acid (MA) treatment of nano-CaO_3 on the crystallization, morphology, and mechanical properties of iPP/nano-$CaCO_3$ composites. They reported that the toughness of PP/MA treated nano-$CaCO_3$ composite was improved drastically. With the addition of 2.5 wt% MA treated nano-$CaCO_3$, the Izod notched impact strength reached its maximum, which was 2.89 times higher than that of pure iPP. More recently, Bao et al.[9] reported that incorporation of functionalized graphene oxide (GO) into iPP can improve the

RSC Advances Accepted Manuscript

impact strength by almost 100%, and the tensile strength by about 30% at a loading of 0.1 wt% functionalized GO. And, Chen et al.[10] reported that the strength and toughness of the final GF/iPP parts were simultaneously improved (tensile strength was increased by 19.3 MPa and the impact toughness by two folds) compared to those of the conventional injection-molded GF/iPP parts. The injection-molded GF/iPP composites had hierachical structure that the outer layer of GF/iPP was dominated by highly oriented glass fibers and shish-kebabs, while the inner layer was dominated by a large population of β-crystals and less oriented glass fibers and shish-kebabs.

For the mechanism of toughenning of iPP by inorganic particles, Kim and Michler[16] proposed the concept of 'three-stage mechanism' for describing the micromechanical deformation processes in various toughened and particle-filled semi-crystalline polymers. The inorganic particles serve as stress concentrators to build up a stress field around themselves. Stress concentration generates triaxial stress around the filler particles and leads to debonding at particle-polymer interface. The voids caused by cavitation or debonding at the particle-matrix interface have occurred. The triaxial tension can be locally released in the surrounding of voids correspinding to an increase in the shear component.

On the other hand, Gersappe[17] suggested, based on the molecular dynamics simulation, that the mobility of nanofillers in polymer controls their ability to dissioate energy, which would increase the toughness of polymer nanocomposites in the case of proper thermodynamic state of the matrix. Zhou et al.[1] experimentally investigated the effect of mobility of non-layered nanoparticles on the toughening of polymers. They investigated mechanical properties of crystalline iPP and amorphous polystyrene (PS) nanocomposites with untreated SiO_2 nanoparticles or grafted SiO_2 nanoparticles at a constant particle concentration of 1.36 vol% at different temperatures. Their results proved that the energy dissipation mechanism induced by nanoparticle mobility works in improving toughness of non-layered nanoparticles/polymer composites.

The mechanical and physical properties of semi-crysalline polymers are also intimately associated with their crystalline features, such as crystal structure, crystalline size, morphology, crystallinity, etc. For example, it is well known that α-form and β-form crystals of iPP exhibit different physical and mechanical properties. The β-form iPP has higher impact toughness, ductility and heat distortion temperature than α-form iPP.[18]

In this work, we fabricated surface attaching silica nanoparticles of silica nanofibers (SiO_2@SNFs) from calcination of electrospun poly (vinyl pyrrolidone)/tetraethyl orthosilicate/silica nanoparticle (PVP/TEOS/SiO_2) nanofibers for toughening of polypropylene (PP). The SiO_2@SNFs had nanoprotrusion structured surface. The degree of surface nanoprotrusion of silica nanofibers (SNFs) was adjusted by incorporated content of SiO_2 nanoparticles. We also investigated effects of SiO_2 content of SiO_2@SNFs on the crystallization behavior, crystal nucleation and mechanical properties of PP.

Experimental

Materials

Poly (vinyl pyrrolidone) (PVP, Mw=130000) and tetraethyl orthosilicate (TEOS) were purchased from Sigma Aldrich Co.. Polypropylene (PP, K8303) was provided from Beijing Yanshan Petrochemical Company, China. Hydrochloric acid solution (37 v/v%), N, N-dimethyformamide (DMF), dimethylsulfoxide (DMSO) and ethanol were purchased from Beijing Eastern Chemical Works, China. The silica (SiO_2) nanoparticles (R974) with 20 nm of diameter were purchased from PPG Industries Inc., USA.

Preparation of solutions for electrospinning

In order to prepare solutions for electrospinning, three kinds of solutions were prepared firstly: (1) PVP solution was prepared by mixing 1.4g PVP, 5.0g DMF, and 2.5g DMSO, (2) TEOS solution was prepared by hydrolyzing the mixed solution of 5g TEOS, 1.5g hydrochloric acid solution (HCl, 37%) and 2.0 g ethanol for 12h, and (3) SiO_2 nanoparticle dispersed solutions were prepared by dispersing a certain SiO_2 nanoparticles in the mixed solvent of 2.0 g DMF and 1.0 g DMSO. And then, three solutions were mixed and stirred for about 24h at room temperature to prepare mixed solutions for electrospinning. The weight ratios of SiO_2/TEOS were 3/100 (3 phr), 6/100 (6phr) and 9/100 (9phr), respectively.

Electrospinning setup

The electrospinning setup was composed of a plastic syringe of 20 ml provided with a needle with the inner diameter of 0.20 mm, a syringe pump (KDS-200), a high voltage power supply (ES30P, Gamma High Voltage Research Inc., USA) and a rotating drum (5 inches of diameter). The operation voltage was 15 kV, the feed rate was 1.0 ml/h, the rotating rate of drum was 300 rpm/min and the distance between needle tip and drum was 20 cm.

Calcination process

The SiO_2@SNFs were obtained by calcination of electrospun PVP/TEOS/SiO_2 nanofibers. The calcination process was performed in a Heavy Duty Tube Furnace (Lindberg 54453) at 325 °C for 6 h, and then at 600 °C for 1 h in order to completely remove organic components. In order to avoid the effect of aspect ratio of SiO_2@SNFs on the mechanical properties of PP, we crushed the SiO_2@SNFs using a pestle in a bowl to obtain short fibers with the length of about 5 μm.

Preparation of PP nanocomposites

The PP/SiO_2@SNFs composites containing 2 wt% SiO_2@SNFs were extruded at 180 °C for twice in order to make uniform mixing at molten state, and then made into pellets at room temperature. To improve the interface bonding between PP matrix and SiO_2@SNFs, γ-methacryloxypropyl trimethoxy silane (KH570) was used as surfactant to modify SiO_2@SNFs. The amount of KH570 was about 10% of SiO_2@SNFs. The samples for impact resistance test were prepared by an injection machine (LMM, Dynisco, Co, USA) using a mould which the size was 3.0 mm (width)×3.0 mm (thickness)×50.0 mm (length) and had a V-shaped gap (0.6 mm of depth and 3 mm of length) in the center. The samples for tensile test were prepared using a dog bone like mould with the length (for narrow section) of 2mm, the width of 2 mm and the thickness of 2 mm.

RSC Advances Accepted Manuscript

 This journal is © The Royal Society of Chemistry 2012

Characterizations

The morphology of nanofibers was characterized by transmission electron microscope (TEM) (Hitachi, H-800 and Tecnai) and scanning electron microscope (SEM) (Hitachi S-4700, Japan). The composition of nanofibers was determined by Fourier transform infrared spectroscopy (FTIR) mounted with a variable incidence angle attenuated total reflection accessory (ATR) (Tensor27, Bruker, Germany). The crystal structure of PP nanocomposites was determined by X-ray diffraction with Cu Kα radiation (40kv and 20mA, D/max2500, Rigaku Co, Japan). The wavelength of X-ray radiation was 0.154 nm and the scan rate was 2 °/min. The crystallization rate of PP nanocomposites was estimated by differential scanning calorimetry (DSC) (Stare system DSC1, Mettler Toledo, Co, Switzerland) under nitrogen atmosphere. In order to observe the melt-crystallization process, the samples were heated at 200 ºC for 5 min to remove thermal history, and then rapidly cooled to 130 ºC to perform isothermal crystallization for 1 hour. The crystalline morphology of PP composites was observed by polarized optical microscope (POM, Leica, Biomed) equipped with temperature controllable hot-stage and photo camera. The tensile tests of PP composites were carried out by a CMT 4102 tensile tester with a cross-head speed of 50 mm/min, and the Notched Izod impact tests were performed by a Resil impactor (Ceast, Italian).

Results and discussion

Formation of nanoprotrusion surface structured SNFs

The SiO_2@SNFs were produced from calcination of electrospun PVP/TEOS/SiO2 nanofibers. In order to understand the structure formation of electrospun PVP/TEOS/SiO_2 nanofibers, the morphology of single electrospun PVP/TEOS/SiO_2 nanofiber was observed by TEM as shown in Figure 1. The electrospun PVP/TEOS/SiO_2 nanofiber showed core-shell structure and had about 450 nm of thickness. The thickness of core and shell were about 230 and 225 nm, respectively.

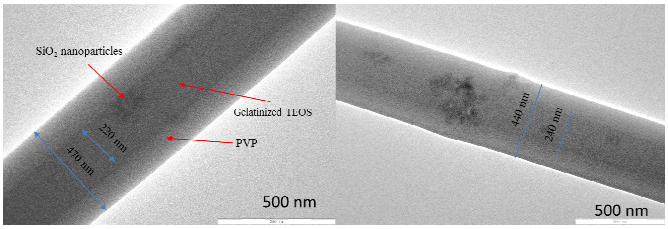

Figure 1. TEM images of single electrospun PVP/TEOS/SiO_2 nanofiber containing 3 phr of SiO_2 nanoparticles.

It indicates that the partial gelatinized TEOS further undergo gelation and phase separation to form the core-shell structured nanofibers during electrospinning process. Based on the contrast of TEM images, we can determine that the gelatinized TEOS and PVP form core and shell of nanofibers, respectively.

The structure changes of PVP/TEOS/SiO_2 nanofiber before and after calcination were characterized by FTIR-ATR method as shown in Figure 2. In the FTIR-ATR spectrum of electrospun PVP/PEOS/SiO_2 nanofibers, the peak at 1625 cm^{-1} assigned to -C=O stretching vibration is contributed from PVP, and the peaks at 3355cm^{-1} assigned to -OH vibrations is contributed from -Si-OH group of gelatinized TEOS. However, the peaks at 1625, 3355 and 948 cm^{-1} of electrospun PVP/PEOS/SiO_2 nanofibers are completely disappeared after calcination. It indicates that the PVP was completely pyrolyzed and gelatinized TEOS was dehydrated during the calcination, and the SiO_2@SNFs were produced by calcination of electrospun PVP/TEOS/SiO_2 nanofibers.

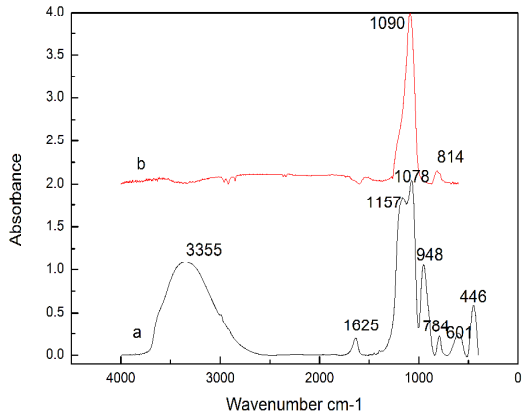

Figure 2. FTIR-ATR spectra of PVP/TEOS/SiO_2 nanofibers containing 9 phr of SiO_2 nanoparticle content (A) before and (B) after calcination.

Figure 3 shows the SEM images of electrospun and after calcination of PVP/TEOS/SiO2 nanofibers containing 9 phr of SiO_2 nanoparticle content. The electrospun PVP/TEOS/SiO_2 nanofibers have smooth surface as shown in Figure 3 (A). After calcination, however, the PVP/TEOS/SiO_2 nanofibers (i.e. SiO_2@SNFs) exhibit nanoprotrusion surface morphology as shown in Figure 3 (B). It is showed by TEM more clearly that somewhat aggregated silica nanoparticles are presented on the surface of SNF as shown in Figure 3 (C). However, the silica nanoparticles are also possible to be embedded in the bulk of silica nanofibers.

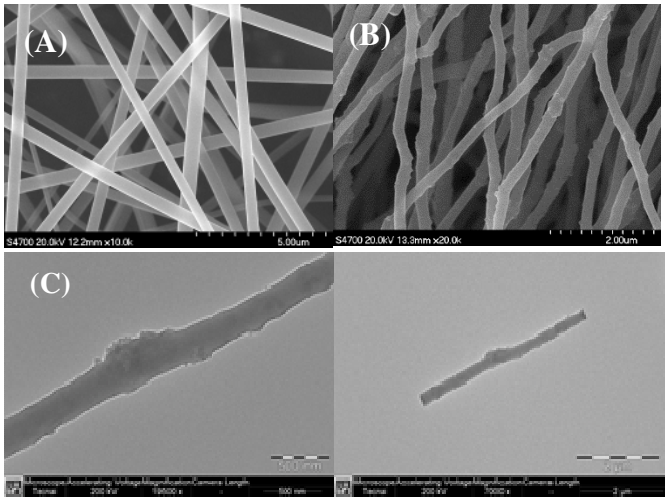

RSC Advances Accepted Manuscript

Figure. 3. SEM images of (A) electrospun and (B) after calcination of PVP/TEOS/SiO_2 nanofibers (i.e. SiO_2@SNFs) containing 9 phr of SiO_2 nanoparticles, (C) TEM images of SiO_2@SNF containing 9 phr of SiO_2 nanoparticles.

The degree of surface nanoprotrusion of SNFs is increased with increase of the incorporated SiO_2 nanoparticles content as shown in Figure 4. However, the precise density of SiO_2 nanoparticles on the SNFs surface is hard to be quantitatively obtain based on the incorporated SiO_2 nanoparticles content in this work due to the uncertain distribution of SiO_2 nanoparticles on the SNFs surface. In spite of this, the degree of surface nanoprotrusion of SNF can be adjusted qualitatively via incorporated SiO2 nanoparticles content of SiO_2@SNFs as shown in Figure 4. The specific surface area and surface roughness of SiO_2@SNFs are influenced by incorporated SiO_2 nanoparticle content. Our previous work[19] showed that the specific surface areas of SiO_2@SNFs were increased to 97.65, 250.52 and 345.07 m^2/g when the incorporation of 1.47, 2.90 and 4.29 wt% of SiO_2 nanoparticles into SNFs, respectively. The surface roughness of SiO_2@SNFs was increased with the increase of the content of SiO_2 nanoparticles.

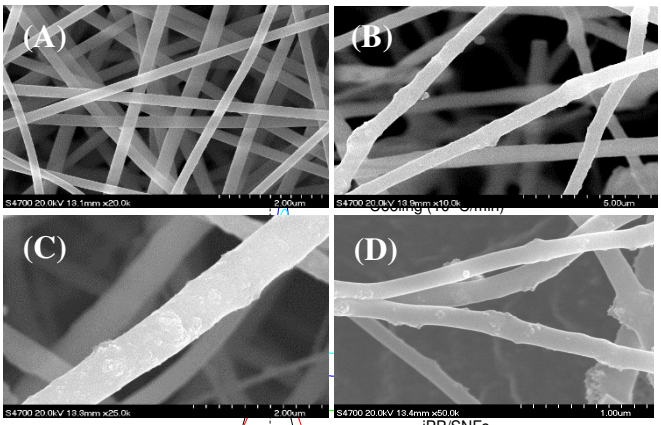

Figure 4. SEM images of SiO_2@SNFs containing various SiO_2 nanoparticles. (A) 0 phr, (B) 3 phr, (C) 6 phr, (D) 9 phr.

Effect of SiO_2@SNFs on the crystal nucleation of PP

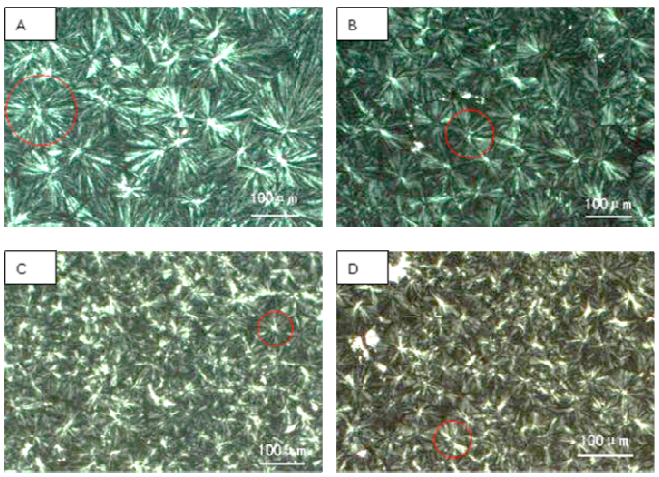

Figure 5. POM images of PP (A) and PP/SiO_2@SNFs nanocomposites containing 2wt% of SiO_2@SNFs with (B) 0 phr, (C) 3phr, and (D) 9phr of SiO_2 nanoparticles obtained at 130 °C.

Effects of SiO_2@SNF on spherulite crystal size and nucleation density of PP were observed by POM. The samples were isothermally melt-crystallized at 130°C for 1 hour. Figure 5 shows that the spherulite crystal size of PP/SiO_2@SNFs composite is obviously decreased as compared with that of pure PP, and slightly decreases with the increase of the content of SiO_2 nanoparticles. Effect of SiO_2@SNFs on crystal nucleation density of PP shows the opposite trend with spherulite crystal size. Those results indicate that the SiO_2@SNFs act as nucleation agent for PP. The spherulite crystal size influences the mechanical properties of PP. In general, the small size of spherulite crystal morphology is favourable for improving the toughness of PP. By comparison with SNF, the SiO_2@SNF showed more effectivity for heterogeneous nucleation of PP.

Figure 6 shows DSC thermograms of PP and PP/SiO_2@SNFs nanocomposites obtained during cooling process with a cooling rate of 10 °C/min. The curves shows that the melt-crystallization temperature of PP is 120.8 °C, and the melt-crystallization temperatures of PP/SiO_2@SNFs composites are 121.5, 122.3, 122.7 and 122.8 °C when the SNFs loading 0, 3, 6 and 9 phr of SiO_2 nanoparticles, respectively. The melt-crystallization temperature of PP was increased with the increase of the SiO_2 content of SiO2@SNFs. It demonstrates that the heterogeneous crystal nucleation of PP can be enhanced by the SiO_2 nanoparticles content of SiO_2@SNFs.

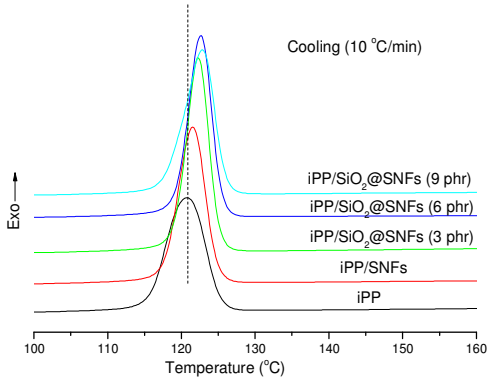

Figure 6. DSC thermograms of PP and PP/SiO_2@SNFs nanocomposites containing 2wt% of SiO_2@SNFs with various SiO_2 nanoparticles (0, 3, 6 and 9 phr) obtained during cooling process with a cooling rate of 10 °C/min.

Effect of SiO_2@SNFs on crystallinity and PP β-form crystal

Effects of SiO_2@SNFs on crystallinity and PP β-form crystal nucleation were determined by XRD as shown in Figure

RSC Advances Accepted Manuscript

This journal is © The Royal Society of Chemistry 2012

7. The diffraction peaks at 2θ=14.2°, 16.2°, 17.0° and 18.6° were observed in the XRD profiles of PP and PP/SiO_2@SNFs nanocomposites. The diffraction peaks at 2θ=14.2°, 17.0° and 18.6° are assigned to the $(110)_\alpha$, $(040)_\alpha$ and $(130)_\alpha$ crystalline planes of PP α-form crystal, and the diffraction peak at 16.2° is assigned to the $(300)_\beta$ crystalline plane of PP β-form crystals. As shown Figure 7, the relative peak intensity of $(300)_\beta$ obviously increases after the incorporation of SNFs into PP. however, the relative peak intensity of $(300)_\beta$ is not further increased by SiO_2@SNFs. It indicates that the relative β-form crystal content of PP is almost uninfluenced by the nanoprotrusion surface morphology of SNFs. The relative β-form crystal content (K_β) of PP can be calculated from X-ray diffraction data according to Turner-Jones et al.[20] proposed equation (1)

$$k_\beta = \frac{H_{\beta(300)}}{H_{\alpha(110)}+H_{\alpha(040)}+H_{\alpha(130)}+H_{\beta(300)}} \quad (1)$$

Where $H_{\alpha(110)}$, $H_{\alpha(040)}$and $H_{\alpha(130)}$ are the intensity of diffraction peaks at 14.2°, 17.0° and 18.8° from iPP α-form crystals, respectively, and $H_{\beta(300)}$ is the intensity of diffraction peak at 16.2° from iPP β-form crystal.

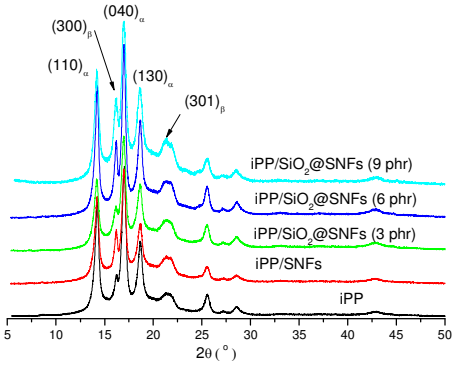

Figure 7. XRD profiles of PP and PP/SiO_2@SNFs nanocomposites containing 2wt% of SiO_2@SNFs with various SiO_2 nanoparticles (0, 3, 6 and 9 phr).

Table 1. Total crystallinity and K_β values of PP/SiO_2@SNFs nanocomposites containing 2 wt% of SiO_2@SNFs with various SiO_2 nanoparticles (0, 3, 6 and 9 phr) .

Sample	X_w	K_β
PP	0.43	0.07
PP/SiO_2@SNFs (0 phr)	0.41	0.12
PP/SiO_2@SNFs (3 phr)	0.43	0.13
PP/SiO_2@SNFs (6 phr)	0.46	0.12
PP/SiO_2@SNFs (9 phr)	0.43	0.14

The total crystallinity can be calculated by the ratio of the total areas of crystal diffraction peaks and whole peaks. The calculated total crystallinity and K_β value are summarized in Table 1. The total crystallinity, X_w (including both of α and β-form crystals) of PP/SiO_2@SNFs nanocomposites is almost independent of the SiO_2 nanoparticles content of SiO_2/SNFs. Even though the K_β value of PP/SiO_2@SNFs composites is almost two times higher than that of PP, the absolute value of K_β is still small. And, the K_β value of PP/SiO_2@SNFs is almost influenced by the SiO_2 nanoparticles content of SNFs. It indicates that the relative β-form crystal content of PP/SiO_2@SNFs composites is insensitive to the degree of surface nanoprotrusion of SNFs. Therefore, effect of PP β-form crystal on toughening of PP may plays minor role in this work due to lower crystalliniy of β-form crystal.

Effects of SiO_2@SNFs on mechanical properties of PP

Figure 8 shows the impact and tensile strength of PP and PP/SiO_2@SNFs at loading 2 wt% SiO_2@SNF with various content of SiO_2 nanoparticles. The impact and tensile strength of PP are 22.0 KJ/m^2 and 25.7 MPa, respectively. The impact strength of PP/SiO_2@SNFs is significantly increased with the increase of the SiO_2 nanoparticles content. For example, the impact strength of PP/SiO_2@SNFs with 9 hpr SiO_2 nanoparticles (41.6 KJ/m^2) is 1.9 time higher than that of PP, even though the SiO_2@SNFs content is only 2 wt%. However, the tensile strength of PP/SiO_2@SNFs composites is almost independent of the SiO_2 nanoparticles content of SiO_2@SNFs.

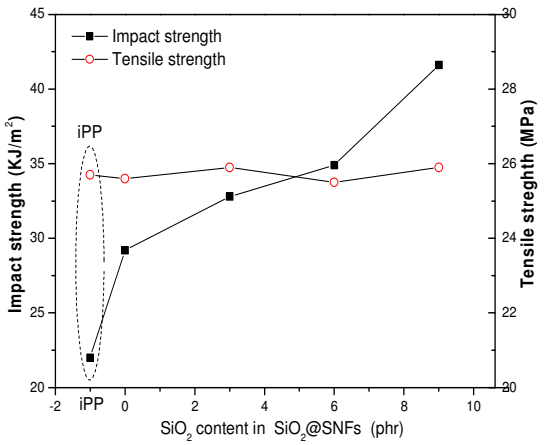

Figure 8. Impact strength and tensile strength of PP and PP/SiO_2@SNFs nanocomposites containing 2 wt% of SiO_2@SNFs with various SiO_2 nanoparticles (0, 3, 6 and 9 phr) obtained at room temperature.

The surface of SiO_2@SNFs was treated with silane (KH570) for improving the interfacial bonding between the fillers and PP matrix. Assuming the interfacial bonding is improved by the silane treatment, and then the applied stress can be transferred from the PP matrix to SiO_2 nanoparticles of SiO_2@SNF during tensile testing. This can lead to an increase in tensile strength with increasing the filler content because the fillers can carry the applied stress. However, Figure 8 shows that the tensile strength of PP/SiO_2@SNFs composites is independent of the

RSC Advances Accepted Manuscript

filler content. The interfacial bonding between the fillers and PP matrix also depends greatly on the amount of silane. Presumably the amount of silane used in this paper is not enough to ensure strong interfacial bonding.

Recently, Zhou et al.[1] reported that mechanical properties of crystalline iPP nanocomposites with untreated SiO_2 nanoparticle and grafted SiO_2 nanoparticle (grafting of poly (dodecafluoroheptyl acrylate), PDFHA, onto the nanoparticles) at a constant particle concentration of 1.36 vol% at different temperatures. Their results showed that the grafted SiO_2 nanoparticle improved the toughening of iPP in contrast with untreated SiO_2 nanoparticle. In their case, the grafted polymer chains on SiO_2 nanoparticle would get entangled with the matrix polymer in the course of melt mixing, leading to improved nanoparticles/matrix interaction, and the fluoride facilitated relative sliding of the grafted nanoparticles under applied stress. Their results proved that the PP composite with energy dissipation mechanism induced by nanoparticle mobility works in improving toughness of non-layered nanoparticles/polymer composites. In our case, the entanglements of PP chains may be enhanced by SiO_2@SNFs due to the rougher surface of SiO_2@SNFs. The SiO_2@SNF in PP matrix shows rougher surface morphology for the containing 9 phr content of SiO_2 nanoparticles than that for containing 3 phr content of SiO_2 nanoparticles as shown Figure 9. It indicates that the nanoprotrusion surface of SNFs promote the interaction between the PP matrix and fillers than SNFs.

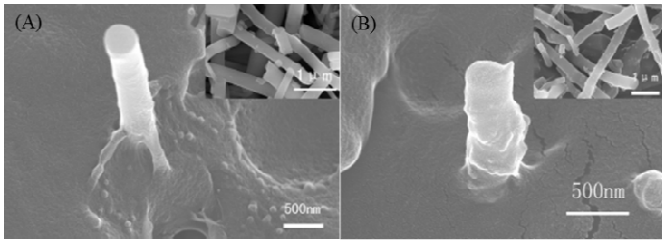

Figure 9. SEM images of PP/SiO_2@SNFs nanocomposites containing 2 wt% of SiO_2@SNFs with various SiO_2 nanoparticles (A): 3 phr, (B): 9 phr. The inserted in (A) and (B) of SEM images are SiO_2/SNFs containing 3 and 9 phr SiO_2 nanoparticles, respectively.

Conclusions

In this work, we successfully fabricated SiO_2@SNFs by calcination of electrospun PVP/TEOS/SiO_2 nanofibers. The SiO_2@SNFs had nanoprotrusion structured surface morphology. The core-shell structured PVP/TEOS/SiO_2 nanofibers were the prerequisite of formation of SiO_2@SNFs. The degree of nanoprotrusion surface of SNFs can be adjusted via the incorporated SiO_2 nanoparticle content. Effects of the SiO_2 content of SNFs on crystallization behaviour, relative content of β-form crystals, and mechanical properties of PP were also investigated. The DSC results indicated that the heterogeneous crystallization nucleation was enhanced by the nanoprotrusion surface structured SNFs. However, the relative content of β-form crystals was almost independent of the SiO_2 nanoparticle content of SiO_2@SNFs. In contrast with SNF, the SiO_2@SNFs provided more improvement of impact strength of PP at same loading content of filler. The impact strength of PP/SiO_2@SNFs at loading 2wt% of SiO_2@SNFs with 9 phr (SiO_2/TEOS=9/100) of SiO_2 nanoparticles was improved 1.9 and 1.4 times than that of neat PP and PP/SNFs composite with 2wt% of SNFs, respectively. Whereas, the crystallinity, relative content of β-form crystal, and tensile strength of PP were almost independent of the SiO_2 nanoparticles content of SNFs. The impact strength of PP can be achieved 41.6 KJ/m^2 at 2 wt% of SiO_2@SNFs with 9 phr of SiO_2 nanoparticles, which can suffice the industrial requirements. The nanoprotrusion surface structured SiO_2@SNFs can promote PP chain entanglements, leading to improve the nanoparticles/matrix interaction. However, the PP β-form crystals plays minor role in the toughening of PP in this work due to lower crystalliniy of β-form crystal. We demonstrated that the nanoprotrusion surface structured silica nanofiber can be used as a novel nanofiller for improving the toughening of PP.

Acknowledgements

The research was supported by the National Basic Research Program of China(2015CB654700 (2015CB674705)), the Fundamental Research Funds for the Central Universities in China (JD1407), the Beijing Higher Education Young Elite Teacher Project (YETP0493), and the Program of Beijing Excellent Talents (2013D009016000003).

Notes and references

[a] College of Materials Science and Engineering, Beijing Key Lab of Special Elastomer Composite Materials, Beijing Institute of Petrochemical Technology, Beijing 102617, P. R. China

[b] State Key Laboratory of Chemical Resource Engineering, Beijing University of Chemical Technology, Beijing 100029, P. R. China

[c] Key Laboratory of Beijing City on Preparation and Processing of Novel Polymer Materials, Beijing University of Chemical Technology, Beijing 100029, P. R. China.

1. T. H. Zhou, W. H. Ruan, M. Z. Rong, M. Q. Zhang and Y. L. Mai, *Advanced Materials*, 2007, **19**, 2667-2671.
2. B. Chen and J. R. G. Evans, *Soft Matter*, 2009, **5**, 3572-3584.
3. J. H. Yang, Y. Zhang and Y. X. Zhang, *Polymer*, 2003, **44**, 5047-5052.
4. Z. Ling, C. Z. Li and H. Rui, *J Polym Sci Pol Phys*, 2005, **43**, 1113-1123.
5. J. I. Weon and H. J. Sue, *J Mater Sci*, 2006, **41**, 2291-2300.
6. L. Li, X. Zhang, F. Luo, Y. Zhao and D. Wang, *Acta Polym Sin*, 2011, **10**, 1218-1223.
7. J. Luo, Y. Liang, J. Yang, H. Niu, J.-Y. Dong and C. C. Han, *Polymer*, 2012, **53**, 2465-2475.
8. Z. Zhang, C. Wang, Y. Meng and K. Mai, *Composites Part A: Applied Science and Manufacturing*, 2012, **43**, 189-197.
9. R.-Y. Bao, J. Cao, Z.-Y. Liu, W. Yang, B.-H. Xie and M.-B. Yang, *Journal of Materials Chemistry*, 2014, **2**, 3190-3199.
10. Y.-H. Chen, Z.-Y. Huang, Z.-M. Li, J.-H. Tang and B. S. Hsiao, *RSC Advances*, 2014, **4**, 14766-14776.
11. E. Igarza, S. G. Pardo, M. J. Abad, J. Cano, M. J. Galante, V. Pettarin and C. Bernal, *Materials and Design*, 2014, **55**, 85-92.
12. N. Tortorella and C. L. Beatty, *Polym Eng Sci*, 2008, **48**, 2098-2110.
13. L. Li and Q. Dou, *Journal of Macromolecular Science, Part B: Physics*, 2011, **50**, 831-945.

RSC Advances Accepted Manuscript

 This journal is © The Royal Society of Chemistry 2012

14. Y. S. Thio, A. S. Argon, R. E. Cohen and M. Weinberg, *Polymer*, 2002, **43**, 3661-3674.
15. Y. Lin, H. Chen, C.-M. Chan and J. Wu, *Macromolecules*, 2008, **41**, 9204-9213.
16. G.-M. Kim and G. H. Michler, *Polymer*, 1998, **39**, 5699-5703.
17. D. Gersappe, *Physical Review Letters*, 2002, **89**, 058301.
18. R. Cermak, M. Obadal, P. Ponizil, M. Polaskova, K. Stoklasa and J. Heckova, *Eur Polym J*, 2006, **42**, 2185-2191.
19. S. Wen, L. Liu, L. Zhang, Q. Chen, L. Zhang and H. Fong, *Materials Letters*, 2000, **64**, 1517-1520.
20. J. A. Turner, J. M. Aizlewood and D. R. Beckett, *Makromolekulare Chemie*, 1964, **75**, 134-158.

RSC Advances Accepted Manuscript